Journal of Nuclear Materials 381 (2008) 152–157

Contents lists available at ScienceDirect

Journal of Nuclear Materials

journal homepage: www.elsevier.com/locate/jnucmat

Microstructural characterisation of nuclear grade graphite

A.N. Jones *, G.N. Hall, M. Joyce, A. Hodgkins, K. Wen, T.J. Marrow, B.J. Marsden

Nuclear Graphite Research Group, Materials Performance Centre, The University of Manchester, P.O. Box 88, Manchester M60 1QD, United Kingdom

A B S T R A C T

Field emission and transmission electron microscopy are used to characterise the microstructure and morphology of baked carbon block and graphitized grades (from the same carbon block stock) of nuclear graphite. Quantitative analysis using Raman and energy dispersive spectroscopy (EDS) were used to investigate the decrease of crystallinity with graphitization and sample purity. Both baked carbon and graphitized nuclear graphites show no sensitivity of the Raman band shift to strain, consistent with strain accommodation by the porous structure.

1. Introduction

Graphite is an attractive choice for a reactor graphite moderator as is it exhibits low coefficient of thermal expansion (CTE), excellent thermal shock resistance and low neutron activation [1]. However, problems may evolve as graphite component dimensions and properties change during operation in the reactors from the effects of fast neutron irradiation and, in the case of carbon dioxide cooled systems, radiolytic oxidation [2–6], which can lead to graphite weight loss and property changes [7,8]. Fast neutron damage causes the graphite crystallites to swell in the '*c*' direction and shrink in the '*a*' direction, leading to bulk dimensional changes. However, in the early stages of irradiation much of the '*c*' direction swelling can be accommodated by internal intra-crystallite porosity. Nuclear graphite internal porosity consists of many pores and cracks ranging from the nano to micro-scale. Their distribution may vary with the choice of raw materials and manufacturing process. As well as dimensional changes other important irradiation induced physical property changes to graphite are changes to the coefficient of thermal expansion (CTE), thermal conductivity, Young's modulus and Poisson's ratio as well as irradiation creep.

The irradiated induced changes to the graphite crystal structure within nuclear graphite have been shown to lead to disruption of the bonding across the basal plane [9] and closure of Mrozowski cracks [10,11], giving similar graphitic structures to that seen before graphitization. It is also known that the elastic modulus and coefficient of thermal expansion of graphite irradiated to a moderate fast neutron dose (40×10^{20} n/cm^2 EDND) are returned to values similar to that of carbon block stock. Specifically, there is an increase in elastic modulus by a factor of about 1.5, an increase in CTE by a factor of about 1.2, and a reduction in thermal conductivity by a factor of about 0.23. In addition, carbon block stock creeps at a lower temperature and at a faster rate than graphite made from the same stock [12,13]. Therefore, to try to understand how these modifications to the crystallite microstructure may influence the properties of nuclear graphite, this paper presents observations on baked carbon block and graphitized grades, from the same carbon block stock, of nuclear graphite. This is a first step towards understanding the influence of the structure on properties. Future studies will investigate irradiated graphite manufactured from the same carbon block stock.

2. Experimental procedures

2.1. Sample preparation

For scanning electron microscope (SEM) and energy dispersive X-ray spectroscopy (EDS) observations, baked carbon and graphitized materials [14] were cleaved and washed in analytical grade ethanol. For transmission electron microscopy (TEM) preparation, baked carbon and graphitized samples were cut to ~3 mm then ground to a thickness of ~30 μm. Samples were glued to 3.05 mm diameter molybdenum TEM discs. Finally, baked carbon and graphitized samples were ion beam thinned to optical transparency using a Gatan PIPs (4 KeV). For the Raman and Deben microstrain testing, baked and graphitized samples were cut to length of 20 mm, width 10 mm and a depth of 3 mm (see Tables 1 and 2).

2.2. Analytical instrumentation

Optical observations were performed using a standard benchtop Olympus BH2 Research Microscope. The electron microscopy observations were obtained on three instruments. For low resolution observations a W-filament scanning electron microscope (Jeol 6300) was employed. High resolution experiments were performed using a Field Emission Gun SEM (Philips XL30) capable of elemental

* Corresponding author. Tel.: +44 161 3062602.
E-mail address: abbie.jones@manchester.ac.uk (A.N. Jones).

0022-3115/$ - see front matter © 2008 Elsevier B.V. All rights reserved.
doi:10.1016/j.jnucmat.2008.07.038

Table 1
EDS analysis of baked carbon samples

Element	Normalised wt%	at.%
Carbon	79.52	82.06
Nitrogen	20.18	17.86
Chlorine	0.14	0.05
Iron	0.09	0.02
Cobalt	0.07	0.01

Table 2
EDS analysis of graphitized samples

Element	Normalised wt%	at.%
Carbon	83.04	85.84
Nitrogen	10.23	9.07
Oxygen	6.37	4.94
Sodium	0.21	0.11
Iron	0.01	0.02
Cobalt	0.13	0.03

analysis with energy dispersive X-ray spectroscopy (Oxford Instruments) and a transmission electron microscope (Tecnai F20). Crystalline purity was ascertained using Raman spectroscopy (Renishaw Ar^+ 2.54 eV, 514 nm). The effect of strain on the Raman response was assessed using a Deben Microtester (Model 3.35). The graphite samples were incrementally loaded under compression to a maximum stress of 41 MPa and Raman spectra were acquired during loading.

3. Results

Fig. 1 shows SEM images of baked carbon and graphitized materials at low magnification. The baked carbon material exhibits a very mixed morphology with large numbers of pores caused by entrapped gases during the manufacturing process, the porosity ascertained using helium porosity experiments is quoted as ~20%, pore sizes were up to 100 μm diameter in size. After graphitization there is an obvious change in structure, the material exhibits areas of oriented morphology, with the graphite crystals aligned and roughly equal in size (~3 μm). There is also a considerable decrease in porosity.

Fig. 2 shows optical images of the baked carbon and graphitized materials. Here it is evident before graphitization that the baked carbon material exhibits a matrix with no clear structure and with a high degree of porosity throughout. Examining the microstructure at higher resolution (Fig. 3) it is evident that the process of graphitization alters the microstructure. The material is dense, with less porosity, and the majority of the graphite crystallites are highly orientated, with few gasification pores apparent.

3.1. EDX analysis

The presence of impurities within both baked carbon and the graphitized samples have been measured using EDS coupled to a FEGSEM. All samples were prepared by fracture. The baked carbon material displayed a matrix containing traces of iron and cobalt, (<1 at.%), as shown in Tables 1 and 2, both of which are very stable carbide formers; small amounts of chlorine were also detected. After graphitization most impurities have been vaporized during the manufacturing process. Although extremely small levels of iron and cobalt remain, it is not clear if these are impurities within the graphites or contaminates from the manufacturing process as they are below the quantitative detection limits of EDX detectors.

3.2. TEM analysis

Fig. 4 shows TEM micrographs of baked carbon. The baked carbon samples show areas of disorder and amorphous carbon, as observed in the FEGSEM images. The high contrast region (indicated by the inset) shows localised areas with crystalline structures. Fig. 4(b) and (c) show the higher magnification TEM images. The

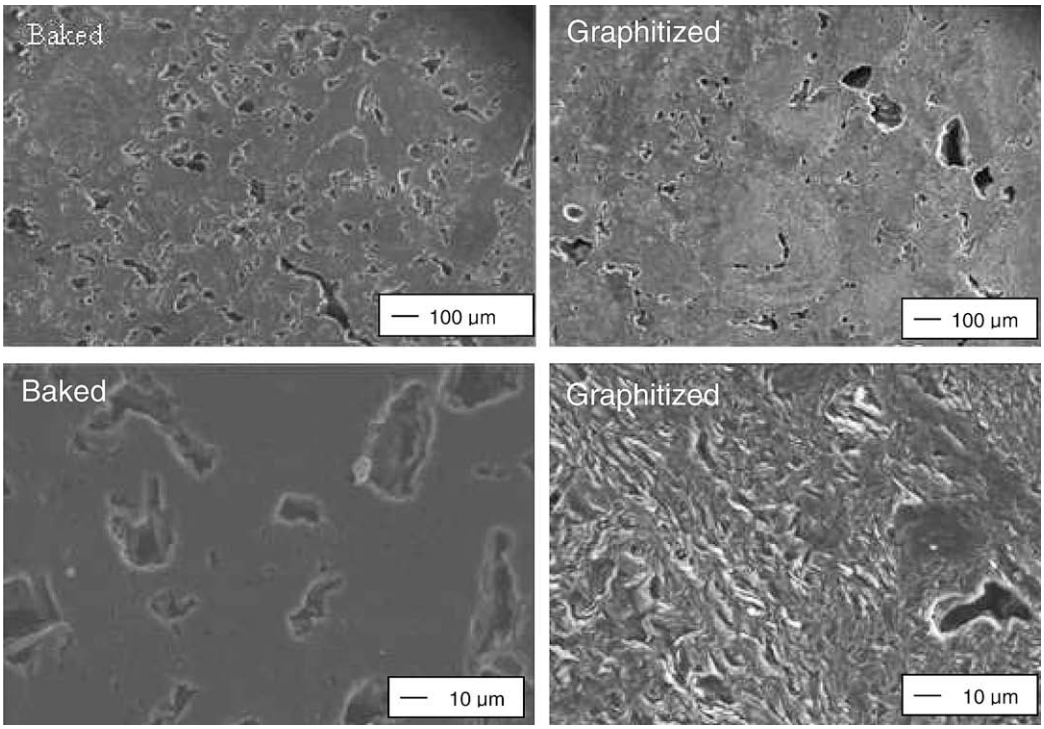

Fig. 1. SEM images of baked carbon and graphitized materials.

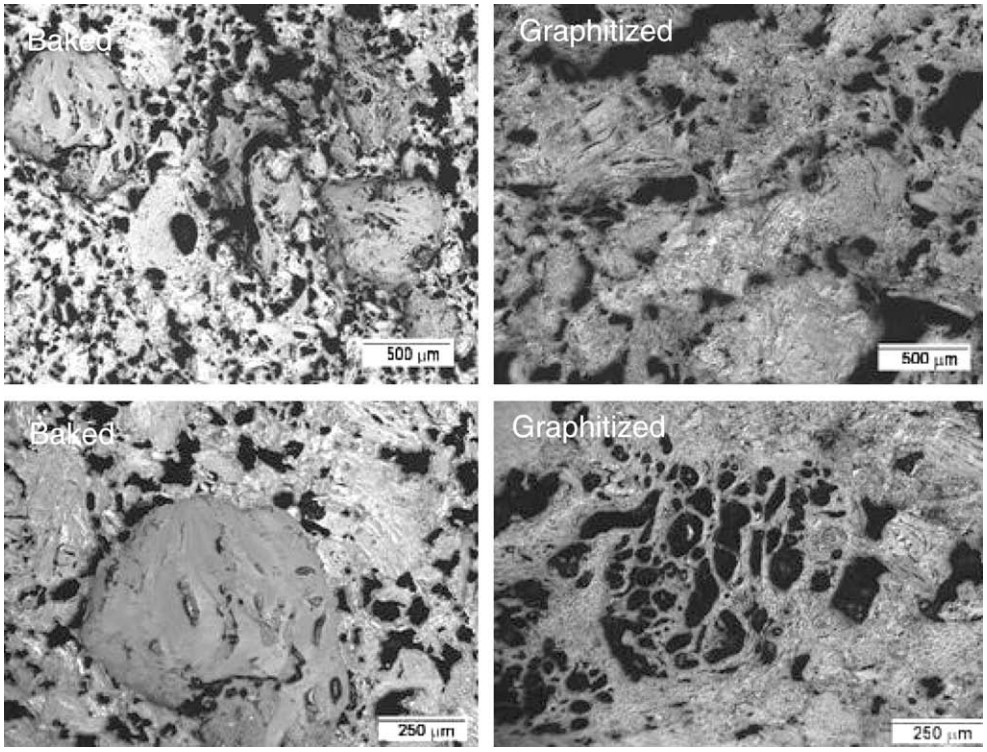

Fig. 2. Optical images of baked carbon and graphitized materials.

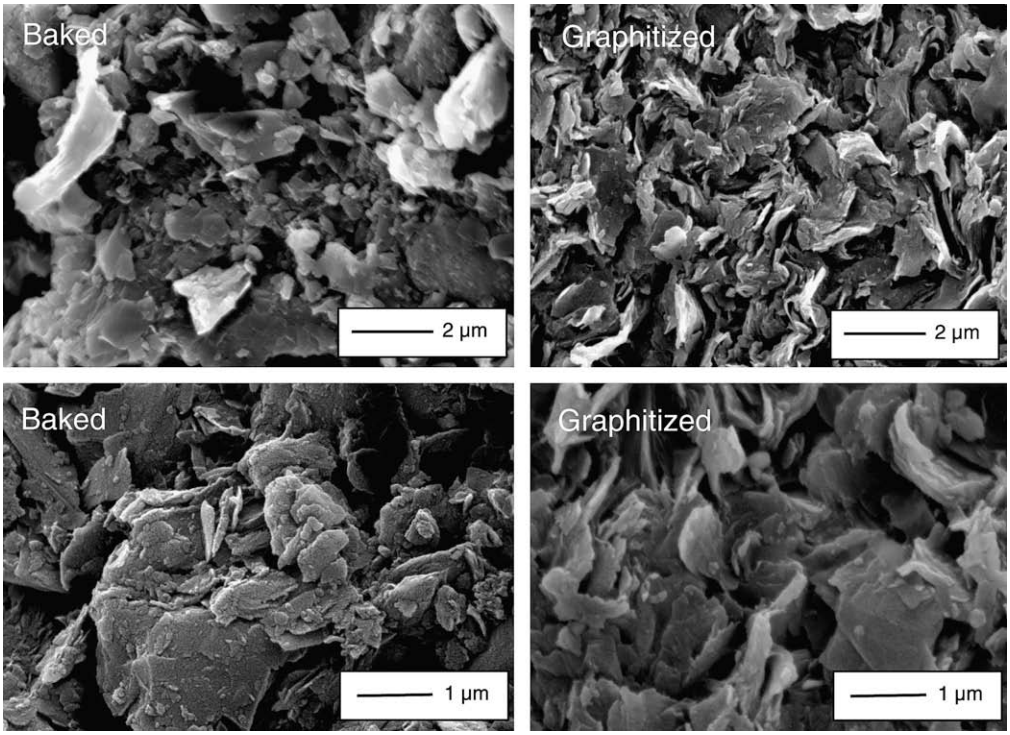

Fig. 3. FEGSEM images of baked carbon and graphitized materials.

graphite structure shows orientated nano-sized graphite crystallites aligned along the disturbed basal planes. During graphitization the structure becomes dense and highly orientated in regions [6]. The microstructural features of graphitized samples are seen in Fig. 5 and the foil shows extensive Mrozowski microcracks. These are considered to form on cooling as the material contracts [10,15]. The cracks are angular, ~30–50 nm width, running parallel to the graphite crystal basal planes. The graphites show local areas of well oriented crystallites, such as those observed in Gilsocarbon nuclear graphites [15] and highly orientated pyrolytic graphites (HOPG) [16]. In the high resolution TEM images in Fig. 4 there are also regions of localised high crystallinity.

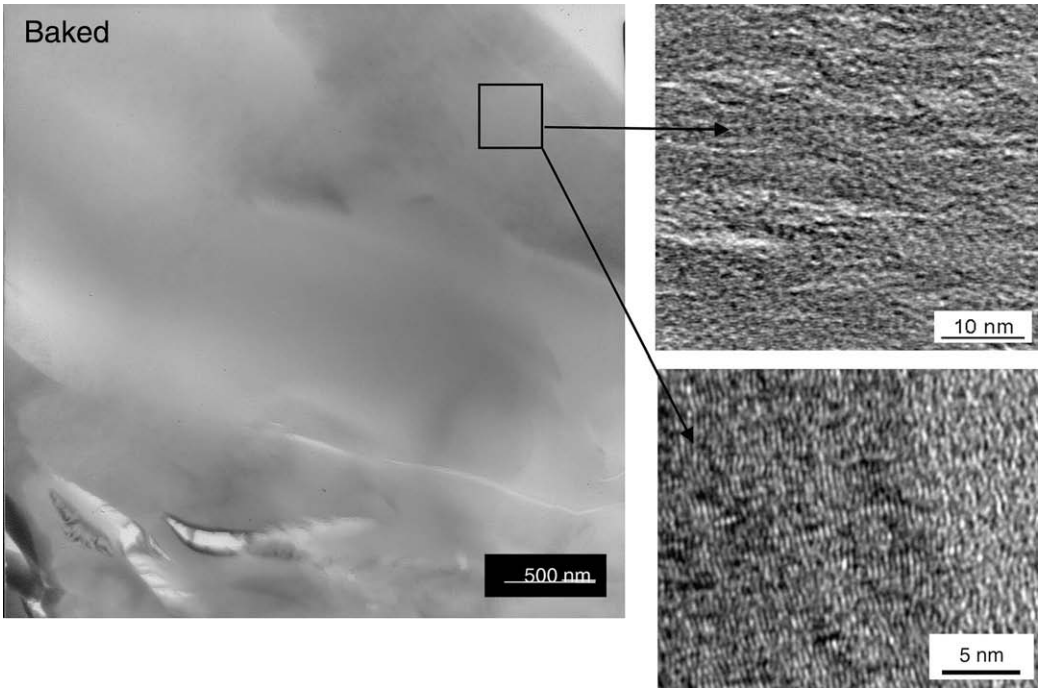

Fig. 4. TEM images of baked carbon graphites.

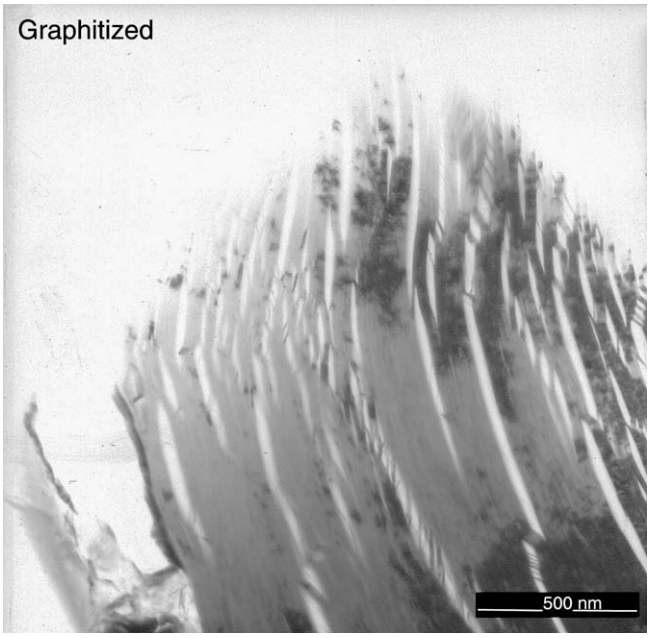

Fig. 5. TEM of graphitized samples.

3.2. Raman analysis

Fig. 6 shows the Raman analysis for a baked carbon block and graphitized. The peak observed at 1340 cm^{-1} is attributed the first order *D*-peak of sp^2 hybridized of carbon phases including disorder carbon, disorder microcrystalline graphite, nanocrystalline graphite or amorphous carbon [17,18]. This peak has also been attributed to the forbidden A_{1g} mode of disordered microcrystalline graphite, which is caused from scattering from the edge to the Brillouim zone due to a size effect of the hexagonal planes in graphite micro-inclusions [17]. The *G*-peak observed at 1580 cm^{-1} is due to

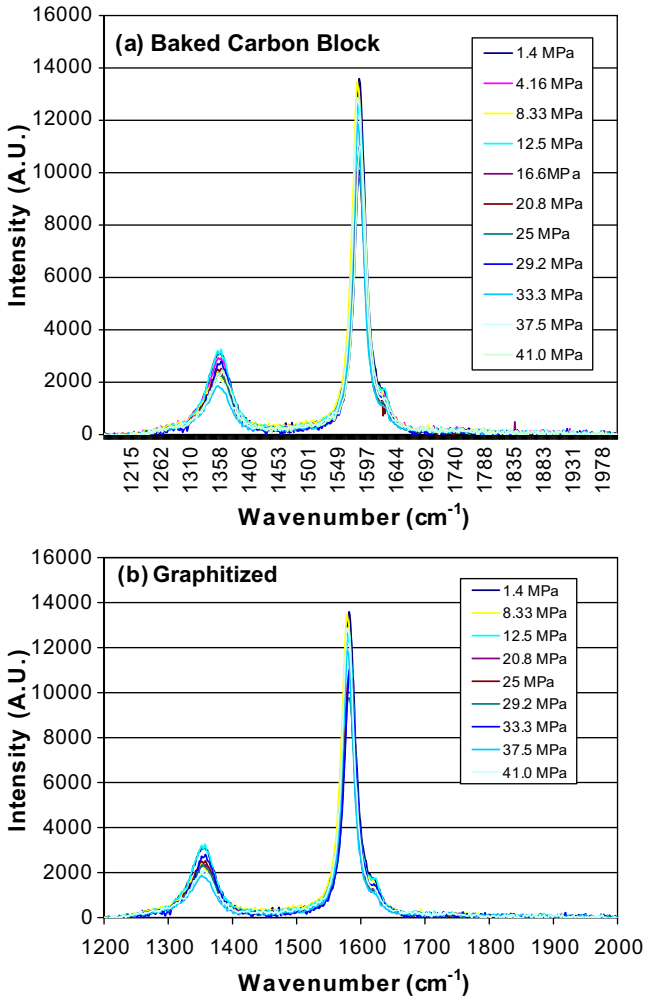

Fig. 6. Raman analysis of baked carbon and graphitized materials under compressive strain.

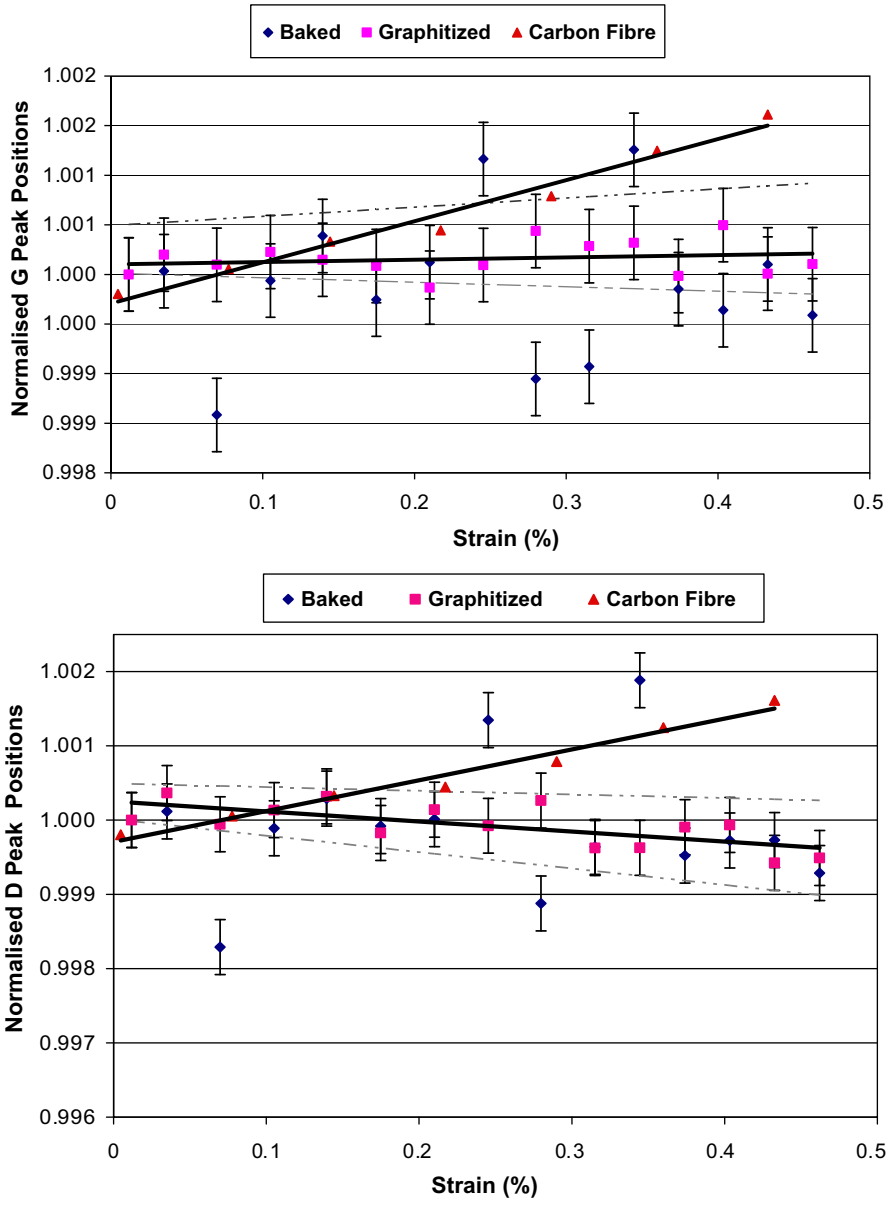

Fig. 7. Normalised Raman frequency shifts as a function of applied compressive strain for baked carbon, graphitized materials and carbon fibre [20].

sp^2 bonded carbon arising from the carbon–carbon double degenerate stretching modes in the hexagonal layers. This is also accompanied with a weak peak at 1610 cm^{-1} assigned to amorphous carbon and/or microcrystalline graphite [19,20].

The strain dependence of graphite materials may be measured at molecular level using Raman Spectroscopy. For graphite fibres it has been found that there is a linear relationship between applied compressive strain and peak shift of about 7 cm^{-1} per 1% elastic strain [21,22] A similar dependence (1.2%) is also observed for nanotubes [26]. The reported variation of peak position with applied strain in compression is typically 30% of that observed in tension [23]. The effects of elastic strain on the normalised *G* and *D-peak* positions for baked carbon and graphitized materials are shown in Fig. 7. The maximum elastic strain applied to both materials was 0.46%. The baked material shows no apparent sensitivity of the *D* and *G*-peaks positions to applied strain. The graphitized material also shows no change in the positions of both the *G* and *D*-normalised peaks with increasing elastic strain.

4. Discussion

The microstructure of the baked carbon block and graphitized material were characterised in terms of crystallinity and porosity using optical and high resolution electron microscopy. The baked carbon block material exhibits a very heterogeneous morphology with areas of disorder and a high degree of porosity. The HRTEM analysis of baked carbon samples shows areas of disorder and amorphous carbon, there are localised areas of crystallisation evident from the disturbed basal planes [24,25]. The microstructure features of graphitized material TEM foils show extensive Mrozowski micro-cracks running parallel to the graphite grains, formed from cooling as the material contracts [15]. Raman analysis shows

strong sp^2 bonding for both the baked carbon and graphitized materials, with evidence of disordered microcrystalline graphite and amorphous carbon. When analysing the Raman spectra for the baked and graphitized materials under compressive strain, It would be expected at any compressive strain may induce a negative shift in wavenumber [26,27]. The compressive stress in *situ* tests show there is no relationship to *D* and *G*-peaks positions with applied strain for baked carbon, this may be explained due to the high degree of inhomogeneity and the lack in definite consistent crystal structure in the baked material and seen in the TEM images (Fig. 4). The graphitized material also shows no deviation from the normalised *D* or *G*-peak position with increasing elastic strain. Given that a significant variation is observed at such strains, this suggests that the applied strain is accommodated by the deformation of the porous structure, without a significant elastic strain developing in the crystalline regions of the graphite.

5. Conclusions

In this paper we have characterised the microstructural features of baked carbon block and graphitized materials from the same stock. HRSEM and TEM were used to examine baked and graphitized materials, TEM analysis shows in the baked material areas of disorder and amorphous carbon. After graphitization there is an obvious change in structure, the graphitized material exhibits areas of oriented morphology and extensive micro cracking is observed. Raman analysis confirms the presence of disordered carbon, disordered microcrystalline and amorphous carbon. Straining experiments show that graphitized material exhibits no deviation from the normalised *D* or *G*-peak position with increasing elastic strain, in comparison to carbon fibres and other crystalline materials. This may indicate a degree of strain accommodation through the pores. The baked material also exhibits no relationship between increasing elastic strain and change in Raman peak position.

Acknowledgements

This work was carried out as part of the TSEC programme KNOO and as such we are grateful to the EPSRC for funding under Grant EP/C549465/1.

References

[1] B.T. Kelly, The Physics of Graphite, Applied Science Publishers, London, 1981.
[2] T.D. Burchell, I.M. Pickup, B. McEnaney, R.G. Cooke, Carbon 24 (1985) 545.
[3] B.T. Kelly, R.E. Taylor, Carbon 6 (1968) 219.
[4] N. Murdie, I.A.S. Edwards, H. Marsh, Carbon 24 (1986) 267.
[5] S.D. Preston, B.J. Marsden, Carbon 44 (2006) 1250.
[6] A.L. Sutton, V.C. Howard, J. Nucl. Mater. 7 (1962) 58.
[7] A.L. Sutton, V.C. Howard, Carbon 1 (1964) 367.
[8] A.L. Sutton, V.C. Howard, J. Nucl. Mater. 7 (1962) 58.
[9] M. Takeuchi, S. Muto, T. Tanabe, H. Kurata, K. Hojou, J. Nucl. Mater. 271–272 (1999) 280.
[10] J.H.W. Simmons, Radiation Damage in Graphite, Oxford, 1965.
[11] B.T. Kelly, W.H. Martin, P.T. Nettley, Philos. Trans. Roy. Soc. Lond. A 260 (1966) 37.
[12] T. Oku, M. Ishihara, Nucl. Eng. Design 227 (2004) 209.
[13] C.L. Mantell, Carbon and Graphite Handbook, Interscience Publishers, New York, 1968.
[14] G.G.S. Products, Technical information UCAR GA and Cs extruded, 2006.
[15] G.M. Jenkins, J. Nucl. Mater. 13 (1964) 33.
[16] S. Muto, T. Tanabe, A. Hirota, M. Rubel, V. Philipps, T. Maruyama, J. Nucl. Mater. 307–311 (2002) 1289.
[17] S.A. Solin, R.J. Nemanich, Phys. Rev. B 20 (1979) 392.
[18] A.M. Zaitsev, Optical Properties of Diamond, Springer, New York, 2001. p. 70.
[19] A.C. Ferrari, Diam. Relat. Mater. 11 (2002) 1053.
[20] J.C. Angus, J.C. Stultz, P.J. Shiller, J.R. MacDonald, M.J. Mirtich, S. Domitz, Thin Solid Films 118 (1984) 311.
[21] C. Galiotis, D.N. Batchelder, J. Mater. Sci. Lett. 7 (1988) 545.
[22] N. Melanitis, P.L. Tetlow, C. Galiotis, S.B. Smith, J. Mater. Sci. Lett. 29 (1999) 786.
[23] N. Melanitis, P.L. Tetlow, C. Galiotis, S.B. Smith, J. Mater. Sci. Lett. 29 (1994) 786.
[24] E. Asari, Carbon 38 (2000) 1857.
[25] E. Asari, Carbon 36 (1998) 1693.
[26] F. Tuinstra, J.L. Koenig, J. Chem. Phys. 53 (1970) 1126.
[27] L.S. Schadler, S.C. Giannaris, P.M. Ajayana, Appl. Phys. Lett. 73 (1998) 3842.